Conserved charged residues at the surface and interface of epithelial sodium channel subunits – roles in cell surface expression and the sodium self-inhibition response

Oded Edelheit[1], Refael Ben-Shahar[1,2], Nathan Dascal[1,3], Aaron Hanukoglu[1,4,5] and Israel Hanukoglu[2]

1 Sackler School of Medicine, Tel-Aviv University, Israel
2 Department of Molecular Biology, Ariel University, Israel
3 Department of Physiology and Pharmacology, Tel-Aviv University, Israel
4 Department of Pediatrics, Tel-Aviv University, Israel
5 Division of Pediatric Endocrinology, E. Wolfson Medical Center, Holon, Israel

The epithelial sodium channel (ENaC) is composed of three homologous subunits that form a triangular pyramid-shaped funnel, anchored in the membrane with a stem of six transmembrane domains. We examined the structure–function relationships of 17 conserved charged residues on the surface of the ectodomain of human γ-ENaC subunit by alanine mutagenesis and co-expression with α- and β-ENaC subunits in *Xenopus* oocytes. The results showed that Na^+ conductance of cells expressing these mutants can be accounted for by two parameters: (a) the ENaC density on the cell surface as measured by the fluorescence of an α-EnaC–yellow fluorescent protein hybrid and (b) the sodium self-inhibition (SSI) response that reflects the open probability of the channel (P_o). Overall, the activity of all 17 mutants was correlated with surface levels of ENaC. There was no significant correlation between these parameters measured for α- and γ-ENaC subunit mutants at nine homologous positions. Thus, the functions of most of the homologous surface residues examined differ between the two subunits. Only four mutants (K328, D510, R514 and E518) significantly reduced the SSI response. The α-ENaC homologs of three of these (R350, E530 and E538) also severely affected the SSI response. The cASIC1 homologs of these (K247, E417, Q421) are located at the interface between subunits, on or about the ion pathway at the rotational symmetry axis in the center of the trimer. Thus, it is likely that these residues are involved in conformational changes that lead to channel constriction and the SSI response upon Na^+ ion flooding.

Introduction

The epithelial sodium channels (ENaC) are located on the apical side of a subset of epithelia in the kidney tubules, respiratory and reproductive tracts, and exocrine glands such as sweat and salivary glands [1,2]. Each ENaC is assembled as a heterotrimer of three homologous proteins termed the α-, β- and γ-ENaC subunits [3,4]. These subunits belong to the ENaC/DEG super-family of voltage-independent sodium channel proteins that include the degenerins found in *Caenorhabditis elegans* participating in mechano-transduction

in neuronal cells, acid-sensing ion channels (ASICs), and mechano-sensitive channels responsible for touch and pain sensation [1,5,6].

All ENaC subunits contain two approximately 20-residue long hydrophobic α-helical segments at their amino and carboxy termini that function as transmembrane (TM) domains anchoring the protein to the membrane [4,7]. The bulk of the ENaC structure is located outside the cell, forming an ectodomain that functions as a funnel to direct ions into the channel pore between the TM domains. Determination of the crystal structure of chicken ASIC1 has contributed greatly to the understanding of the ENaC structure [8–10]. Modeling studies and sequence homology among subunits suggest that the structural domains observed in ASIC are mostly conserved in ENaC [4,5]. Yet, in contrast to ASIC that can function as a homotrimer of identical subunits, ENaC is an obligate heterotrimer [3,4]. A mutagenesis study suggests that the clockwise orientation of the subunits is αγβ (as viewed from the top of the ectodomain) [11].

Genetics of the hereditary multi-system pseudohypoaldosteronism that results from mutations in ENaC subunits demonstrated that all three subunits are essential for ENaC function [12–16]. *In vitro*, full activity of ENaC is observed only when all three subunits are co-expressed [3,17]. Studies expressing mutated ENaC subunits in *Xenopus* oocytes have demonstrated that the ion conductance activity of ENaC in oocytes is correlated with the severity of the phenotype of multi-system pseudohypoaldosteronism [14,16]. These results suggest that ENaC activity in oocytes reflects the physiological activity of ENaC in human tissues.

ENaC comprises part of the complex physiological systems that regulate extracellular fluid and blood volume and consequently blood pressure [18,19]. Accordingly, ENaC activity is regulated by a complex array of hormones and extracellular factors [20,21]. These factors can modulate, directly or indirectly, two major parameters that determine ENaC Na^+ conductance: (a) the number of channels in the apical membrane and (b) the open probability (P_o) of the channels [20,21]. In oocytes expressing mutated α-ENaC subunits, we estimated these two parameters by measuring: (a) the fluorescence of yellow fluorescent protein (YFP) labeled γ-ENaC subunit at the oocyte membrane and (b) the sodium self-inhibition (SSI) response of ENaC [3] that reflects channel P_o [22–25]. Although some mutants mainly affected the surface density of the channels, others affected the SSI response. The final macroscopic Na^+ conductance generated by each ENaC mutant could be accounted for by a combination of the values of these two parameters [3].

The present study was undertaken to examine the functions of conserved charged residues on the surface of ENaC subunits. Because ENaC ectodomain is exposed on the cell surface and functions as an ion channel, surface-exposed charged residues provide the surface charge essential for its solubility in the extracellular milieu and the interactions with ions in its environment. Beyond such nonspecific electrostatic interactions, depending on their positions, charged residues may have multiple roles. Residues on the subunit surface may be involved in subunit–subunit binding, interactions with other molecules that may regulate ENaC activity or intracellular trafficking, as well as guidance of ions by electrostatic attraction or repulsion. Because we examined conserved charged residues, these are more likely to fulfil specific roles rather than just nonspecific ionic interactions. In the present study, we selected charged residues that are predicted to be on the ENaC surface, based on ASIC1 models. The rationale for this choice was based on two main considerations: (a) surface residues are more likely to be involved in the protein–protein interactions that we are interested in identifying and (b) alanine mutagenesis of residues protruding on protein surface is less likely to lead to major three-dimensional conformational changes in the interior of the protein that would confound any clarification of the function of the mutated residue.

For the present study, we selected two groups of charged residues: (a) residues located on the exposed surface and (b) residues located at subunit–subunit interface based on ASIC models. In large sets of protein structures, conserved residues are commonly found at protein–protein interaction surfaces [26–28]. We examined the effects of alanine mutants on the two parameters vital to ENaC function noted above: cell surface expression and the SSI response of ENaC that reflects channel P_o. The results obtained revealed that all charged residues located at subunit interface affected at least one of these parameters. By contrast, none of the mutated residues on the exposed surface of ENaC had any effect on the SSI time constant. These results provide evidence that the SSI response is dependent on subunit–subunit interaction sites but not sites on the exposed ENaC surface that were mutated.

An additional question examined in the present study relates to the symmetrical organization of the ENaC subunits. In the structure of ASIC1 composed of three identical subunits, there is a three-fold symmetry in the positions of most residues within the trimeric complex, especially in the ectodomain [8]. If there is a three-fold symmetry among ENaC subunits, we could

expect similar results from mutagenesis of homologous residues in different subunits. In previous structure–function studies of ENaC, evidence has been provided for both symmetrical and asymmetric organization of homologous residues in different ENaC subunits [29,30]. Nine of the residues examined in the present study in γ-ENaC are homologous to previously mutated residues in the α-ENaC subunit that shares approximately 30% homology with γ-ENaC. A comparison of the findings for both subunits shows that there are major differences in the functions of homologous residues in both subunits.

Results

We selected 17 residues in the ectodomain of γ-ENaC for alanine mutagenesis that are conserved in all known sequences of γ-ENaC from eight species (human, bovine, guinea pig, mouse, rat, rabbit,

chicken and *Xenopus*). An additional criterion was representation of the secondary structural domains of the ENaC ectodomain based on sequence, structural and functional comparisons with the chicken ASIC1 models [8,10] (Fig. 1 and Table 1). The proximal region of the γ-ENaC ectodomain contains a consensus motif RXXR for cleavage by protease furin [31,32]. The residues that we selected were distal to this sequence.

Effect of alanine mutagenesis on ENaC activity

To assess the effect of the alanine mutagenesis of residues on ENaC activity, we expressed wild-type (WT) α- and β-ENaC together with mutated γ-ENaC in *Xenopus* oocytes and used the two-electrode voltage-clamp method to assay Na^+ conductance as described in the Experimental procedures. Nine of the 17 γ-ENaC mutations caused a significant
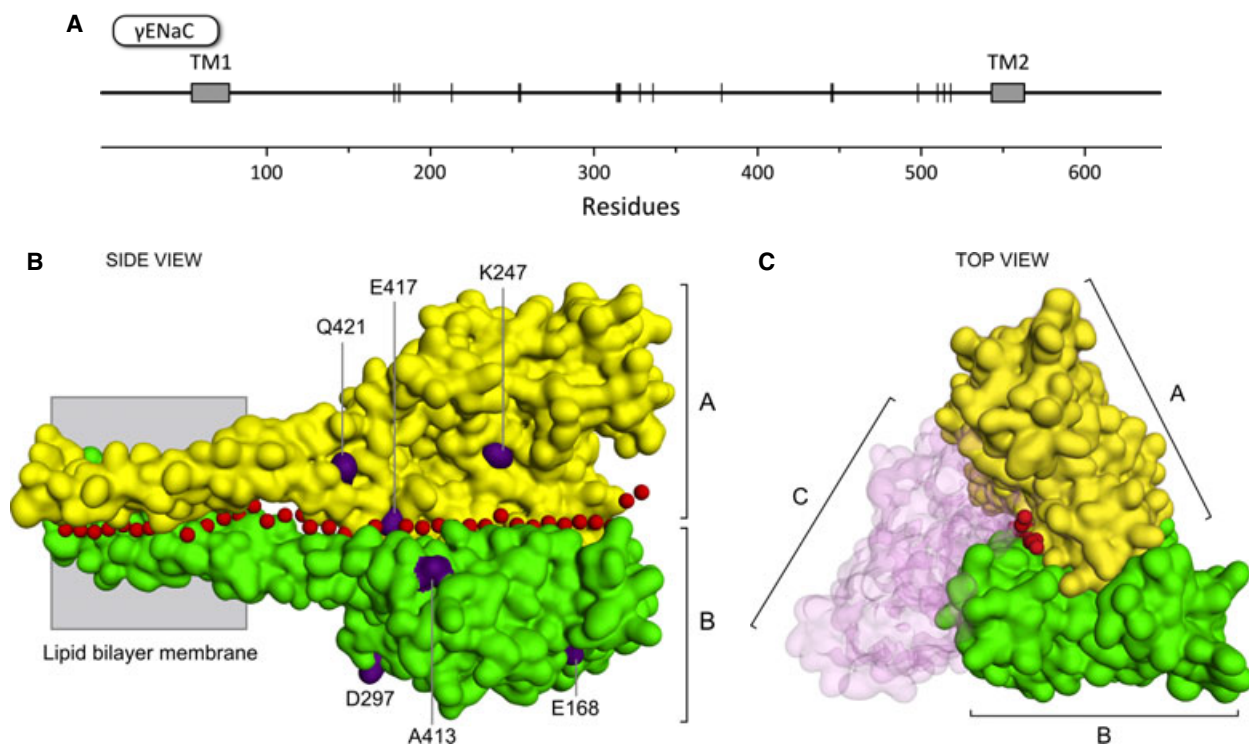

Fig. 1. Positions of the conserved charged residues mutated to Ala. (A) Positions of the residues in the primary structure of human γ-ENaC subunit (SCNNG_HUMAN in UniProt database). TM1 and TM2 mark the amino and carboxy terminal trans-membrane segments of the subunit. The N and the C termini are located in the cytoplasm, and the portion between TM1 and TM2 is the extracellular domain. (B) Side view of the surfaces of A and B subunits of chicken ASIC1 (PDB 2QTS). Surfaces of the homologous residues in the tertiary structure of ASIC1 (Table 1) that are visible in this view are marked in purple. The four hydrophobic helices of the A and B subunits are embedded in the lipid bilayer marked by gray shading. The third subunit (C) surface is not shown to allow visibility of the central pore predicted by the POREWALKER software [50]. Red colored small spheres represent water molecules placed at the center of the predicted pore in each 3 Å slice of 2QTS calculated by POREWALKER. (C) Top view of the three subunits (A, B and C) of ASIC1. Subunit C is shown as a transparent surface to allow visibility of the surfaces of A and B subunits and the predicted pore marked by water molecules as noted in (B).

decrease in Na$^+$ conductance relative to WT ENaC activity (Fig. 2). The most severe inhibition of ENaC activity was observed for E255 (12% of WT

Table 1. Alanine mutated conserved charged residues in γ-ENaC and locations of homologous residues in ASIC1 secondary structural domains.

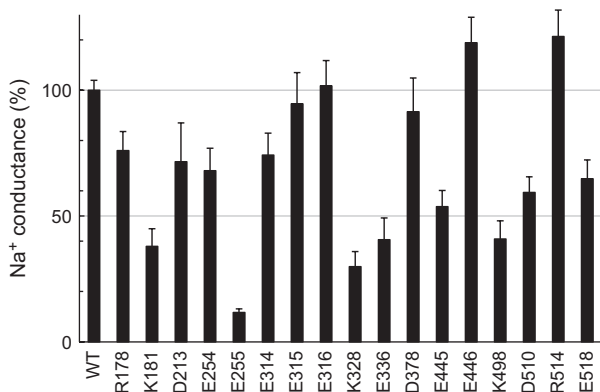| γ-ENaC residue	Conserved in subunits	α-ENaC	cASIC1	ASIC1 secondary structural domain	ASIC1 domain
R178	αγ	R202	–		
K181	γ	S205	–		
D213	αγ	D235	K142	α2–α3	Finger
E254	βγ	G276	–	α3–β3	ERD
E255	γ	N277	E168	α3–β3	ERD
E314	γ	Q336	Q227	β6–β7	Palm
E315	βγ	N337	D228	β6–β7	Palm
E316	αβγ	D338	E229	β6–β7	Palm
K328	αβγ	R350	K247	β7	β-ball
E336	αγ	E358	E255	β7–β8	β-ball
D378	αγ	D400	D297	β9–α4	Thumb
E445	αγ	D467	E354	α5	Thumb
E446	βγ	H468	K355	α5–β10	Thumb
K498	αβγ	R518	–	α7	Knuckle
D510	αβγ	E530	A413	β11–β12	Palm
R514	αβγ	K534	E417	β12	Palm
E518	αβγ	E538	Q421	β12	Palm

Fig. 2. ENaC Na$^+$ conductance in oocytes co-expressing α-, β- and γ-ENaC subunits with a charged residue mutated to Ala. Results represent Na$^+$ conductance in oocytes injected with WT cRNAs for α- and β-ENaC and γ-ENaC cRNA carrying a single residue mutated to Ala (WT without a mutation). The amiloride-sensitive sodium current was measured by the two-electrode voltage clamp method 24 h after injection. Results were normalized relative to sodium conductance measured in oocytes injected with WT cRNAs for α-, β- and γ-ENaC (WT), which was taken as 100%. The results shown are the mean ± SEM of at least 13 oocytes per mutation. For the following mutants, the mean was significantly different from the WT: K181, E255, E314, K328, E336, E445, K498, D510 and E518 ($P < 0.01$ for all except for E314).

activity) and K328 (22% of WT activity) mutants (Fig. 2).

As previously shown for α-ENaC [3], the decrease in macroscopic Na$^+$ conductance with γ-ENaC mutants could be accounted for by a decrease in the surface expression of ENaC or an enhanced SSI response reflecting a decrease in channel P_o. To distinguish between these two effects, we determined both of these parameters for each mutant as described below.

Na$^+$ conductance activity is correlated with the oocyte surface density of ENaC

In our previous study on α-ENaC, we showed that mutation of specific conserved charged residues to alanine may affect the surface density of ENaC, and that there is a high degree of correlation ($r = 0.87$) between ENaC Na$^+$ conductance activity and the surface density of ENaC (as measured by fluorescence of the γ-ENaC–YFP hybrid on the oocyte membrane under confocal microscopy) [3]. Therefore, in the present study of γ-ENaC, we first examined whether a similar correlation would be observed for γ-ENaC mutants as well.

Surface expression of ENaC containing α-ENaC mutants was monitored using a γ-ENaC–YFP hybrid construct [3]. Because we planned to study the effect of γ-ENaC mutants, the use of the γ-ENaC–YFP hybrid could complicate both the generation of mutants and any interpretation of the results. Therefore, instead of the γ-ENaC–YFP hybrid, we generated an α-ENaC–YFP hybrid construct to be used as a fluorescent reporter of membrane levels. In control experiments, we verified that that the fusion of YFP to the carboxy terminal end of α-ENaC did not adversely affect ENaC activity. We then coexpressed the mutated γ-ENaC with α-ENaC–YFP. It should be noted that this approach has been validated by earlier findings showing that all three subunits are required for surface expression and that the absence of one subunit leads to scarcely detectable levels of surface expression [3].

Membrane fluorescence of α-ENaC–YFP (Figs 3 and 4) showed significant correlation with the macroscopic Na$^+$ conductance of 17 mutants of γ-ENaC (Fig. 5) ($r = 0.77$). The two γ-ENaC mutants (E255A and K328A) showing the most severe inhibitory effect on ENaC activity also showed the lowest level of membrane fluorescence (Figs 2 and 4).

Nine of the residues previously mutated in α-ENaC are homologs of the residues mutated in γ-ENaC. A comparison of the two sets of surface level data for
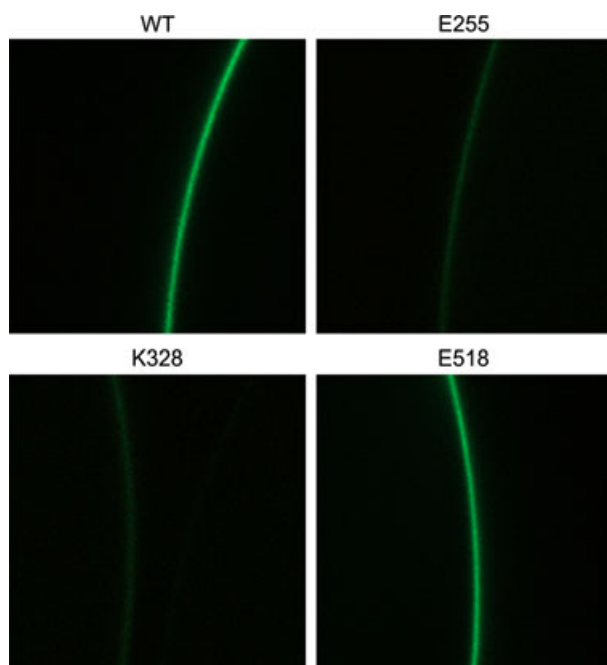
Fig. 3. Fluorescence micrographs of α-ENaC–YFP hybrid protein expressed together with β- and γ-ENaC subunits in the animal (dark) hemisphere surface of *Xenopus* oocytes. Oocytes were injected either with WT or mutated γ-ENAC cRNAs where the indicated γ-ENAC residue was mutated to alanine. For other details, see Experimental procedures. The illustrative samples represent the E255A and K328A mutants that showed the greatest reduction of surface fluorescence and the E518A mutant that did not significantly affect surface expression as shown in Fig. 4.
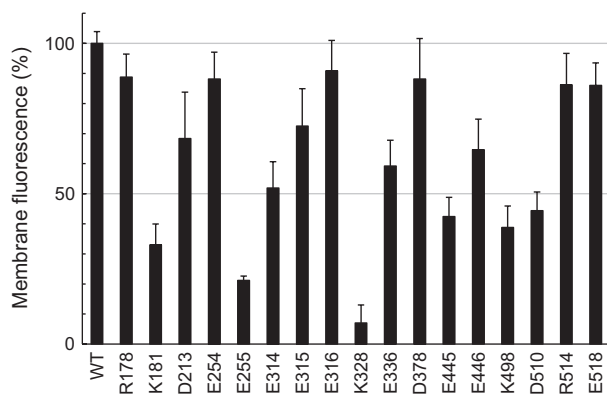
these nine homologs from α- and γ-ENaC did not show a quantitative correlation in their effect on surface expression levels (Fig. 6). The greatest difference was
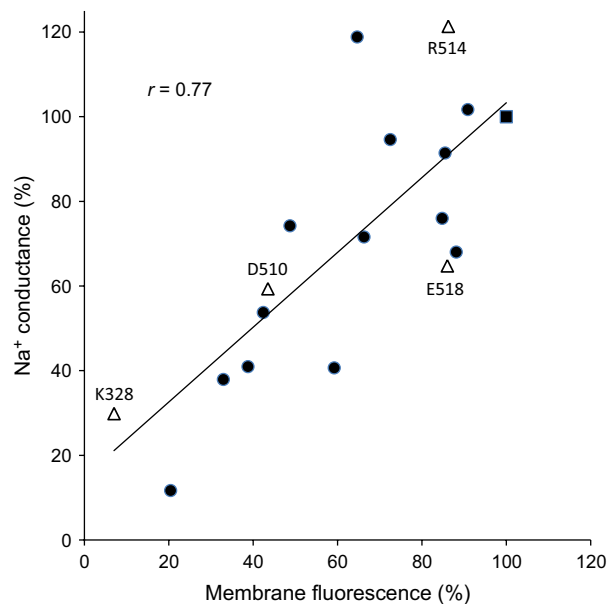
Fig. 5. Correlation of Na⁺ conductance with oocyte cell surface fluorescence of ENaC. The points are taken from the results of the experiments shown in Figs 2 and 4. The Pearson correlation coefficient is $r = 0.77$ ($P < 0.0001$). The four points marked with a triangle represent the results for four residues that had a significant effect on the SSI time constant. The square represents WT.

Fig. 4. Cell surface intensity of fluorescence of α-ENaC–YFP hybrid protein expressed together with β- and γ-ENaC subunits in *Xenopus* oocytes. The residue noted at the bottom of each bar marks the residue of γ-ENaC that was mutated to alanine. Each bar represents the mean ± SEM of at least ten oocytes per residue. The fluorescence intensity was measured as noted in the Experimental procedures. For the following mutants, the mean was significantly different from the WT: K181, E255, E314, K328, E336, E445, E446, K498 and D510 ($P < 0.01$ for all except for E446).

Fig. 6. Comparison of the effects of homologous α-ENaC and γ-ENaC mutants on membrane fluorescence of ENaC. Each paired result represents the alanine mutant of two homologous residues in α-ENaC (upper row of labels) and γ-ENaC (lower row of labels), respectively. The results for α-ENaC were taken from our previous study [3].

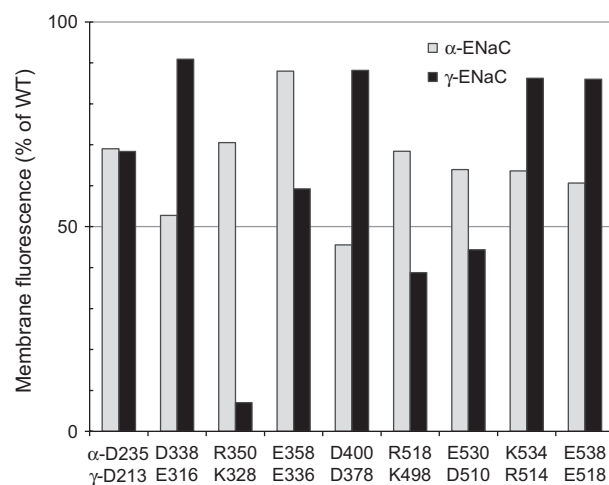observed between R350A mutant for α-ENaC versus homologous K328A mutant in γ-ENaC (Fig. 6).

Effect of alanine mutagenesis on the SSI response of ENaC

Previous studies demonstrated that mutations of conserved residues can affect the SSI response of ENaC [3,23,30,33]. To determine whether there was a correlation between Na$^+$ conductance and the self-inhibition response, we determined the SSI response time constant (τ) for all mutants. Comparison of the Na$^+$ conductance and τ did not show a significant correlation between these two parameters (Figs 2 and 7).

Alanine mutagenesis of only four residues (K328, D510, R514 and E518) out of 17 residues mutated caused a significant change in τ relative to WT ENaC (Fig. 7). In all four cases, τ was increased. In other words, in these four mutants, the SSI response was reduced. Representative recordings of the self-inhibition response (current decay) are provided to illustrate this reduction (Fig. 7). As seen in the recording for the WT in Fig. 7, within 10–20 s after flow of Na$^+$ into the cell, the current decreases sharply and reaches a new plateau. This rapid reduction of current reflects the SSI response [25,34]. The greatest reduction of self-inhibition was observed for the D510A mutant. As seen in the first recording for D510 mutant, in 24 of the 29 oocytes measured, τ could not be calculated because there was no self-inhibition. For the remaining five oocytes that showed low but detectable self-inhibition (as seen in the second sample recording for D510), the mean τ value was 361 ± 71 relative to WT (Fig. 7).

As an additional measure of the mutation effect on ENaC function, we also measured the ratio of steady-state to peak current (I_{ss}/I_{peak}) for all mutants (Fig. 8). The correlation between τ and I_{ss}/I_{peak} was 0.68 for all residues. As noted above, τ was increased in four mutants: K328A, D510A, R514A and E518A. The I_{ss}/I_{peak} values for the first three of these (K328, D510, R514) were significantly higher than WT ($P < 0.01$, $P < 0.01$ and $P < 0.05$, respectively). One additional mutant (K181A) also showed an I_{ss}/I_{peak} higher than WT, although τ was not significantly different from WT. Four additional mutants (R178, D213, E254 and E315) showed an I_{ss}/I_{peak} significantly lower than WT (Fig. 8).

Co-expression of α-ENaC and γ-ENaC with homologous mutations

To examine the function of homologous residues, we concentrated on two residues of γ-ENaC (K328 and D510) that showed strongly adverse effects on both
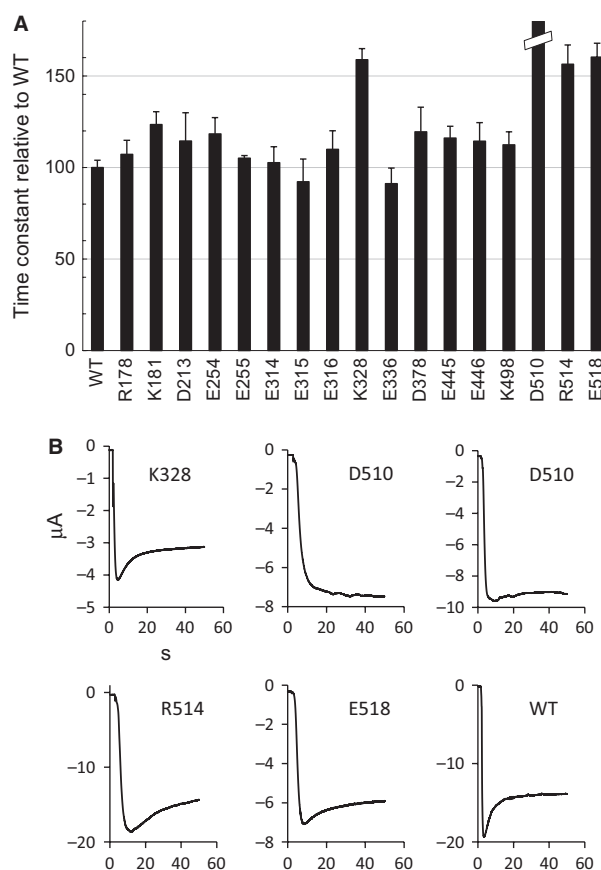

Fig. 7. Effect of mutation of γ-ENaC charged residues to Ala on the SSI response of ENaC. (A) Oocytes were injected with WT cRNAs for α- and β-ENaC and mutated γ-ENaC cRNA carrying a single residue mutated to Ala (WT without a mutation). In each experiment, oocyte was clamped at −60 mV and whole cell current was recorded when superfusing with medium containing 1 mM NaCl. [Na$^+$] was then increased rapidly to 33 mM. The time constant value τ for current decay was determined for a period of 40 s starting with the peak response of each recording as noted in the Experimental procedures. Results are shown relative to WT control oocytes of each batch. Each bar represents the mean ± SEM of at least 10 oocytes except for D510. (B) Representative recordings of the self-inhibition response (current decay) are shown only for four mutants (K328, D510, R514 and E518) that showed τ values significantly different ($P < 0.01$) from the WT ENaC. For D510A mutant, we examined 29 oocytes. For 24 of these, time constant τ could not be calculated because there was no self-inhibition as seen in the first sample recording for D510. Only five oocytes showed low but detectable self-inhibition as seen in the second sample recording for D510. The mean ± SEM for these five oocytes was 361 ± 71 relative to WT. In all recordings, the y-axis units is current (*I*) in μA, and the x-axis unit is time in seconds.

Na$^+$ conductance and the self-inhibition response of ENaC (Figs 2 and 7). The homologs of these two residues in α-ENaC are R350 and E530 (Table 1). In our

previous study on α-ENaC, both R350A and E530A mutants most strongly affected self-inhibition [3]. When expressed alone, without other mutants, alanine mutants of these two homologous residues in α and γ subunits significantly inhibited the Na^+ conductance of
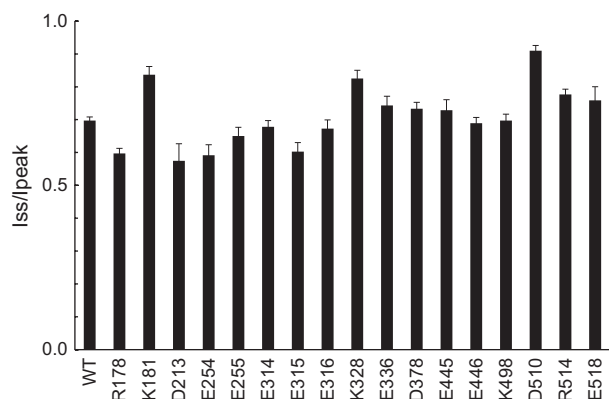

Fig. 8. Effect of mutation of γ-ENaC charged residues to Ala on the I_{ss}/I_{peak} ratio during the SSI response of ENaC. For experimental details, see the legend to Fig. 7.
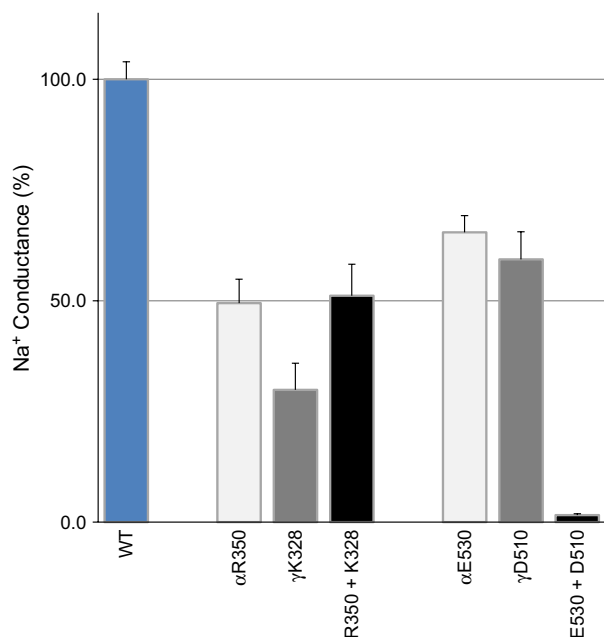

Fig. 9. Na^+ conductance in oocytes expressing α- and γ-ENaC subunits with homologous charged residues mutated to Ala. Oocytes were injected with WT cRNA for β-ENaC and α- and γ-ENaC cRNAs carrying a single residue mutated to Ala (WT without a mutation). For experimental details, see the legend to Fig. 2. Na^+ conductance in oocytes co-expressing both mutated α-and γ-ENaC subunits (αR350 + γK328 and αE530 + γD510) was significantly different from the WT ($P < 0.001$).

ENaC, reducing it to between 30% and 65% of the WT value (Fig. 9). When co-expressed, the homologous pair α-R350 + γ-K328 mutants resulted in approximately 50% inhibition, which is similar to the inhibition observed with each mutant alone (Fig. 9). By contrast, co-expression of the α-E530 + γ-D510 mutant pair resulted in a drastic reduction of Na^+ conductance to approximately 2% of WT (Fig. 9). These results showed that the pair of residues (α-E530 + γ-D510) represents a domain vital for ENaC function.

The results of the SSI time constant measurements for the homologous pairs are shown in Fig. 10. When expressed alone, the α-R350 and γ-K328 mutants showed contrasting behaviors. Although the α-R350A mutant decreased τ (i.e. increased self-inhibition), the corresponding γ-K328A mutant increased τ (i.e. decreased self-inhibition) relative to WT values. The results for the co-expressed pair α-R350A + γ-K328A mutant showed a behavior between the two contrasting values. These results indicate that the two contrasting effects apparently compensated for one another, yielding a mean value close to normal (Fig. 10).

The second homologous pair of residues (α-E530 and γ-D510) showed a consistent behavior when expressed alone because each mutant increased τ to > 170% of WT values (Fig. 10). In oocytes co-expressing both of these mutants, the self-inhibition could not be reliably measured because of the low Na^+ conductance (see sample recording in Fig. 10). Overall, these results indicate that this pair of residues is critically important for both Na^+ conductance and the self-inhibitory response of ENaC.

A summary of results

In Table 2, we summarize the significant effects of alanine mutagenesis. Based on the results obtained with the γ-ENaC alanine mutants, three distinct groups of residues emerged in terms of their effects on ENaC expression and function: (a) residues that affect surface expression; (b) residues that affect the SSI time constant; and (c) residues that affect both parameters (Table 2).

As noted above, according to the homologous ASIC1 structure, we had selected conserved residues located at the exposed surface, as well as at the interface between subunits. All the mutated residues located at interface affected adversely either cell surface expression or SSI. By contrast, the mutant residues that had no effect on either of these parameters are located on the exposed surface of the ASIC1 model (Table 2).
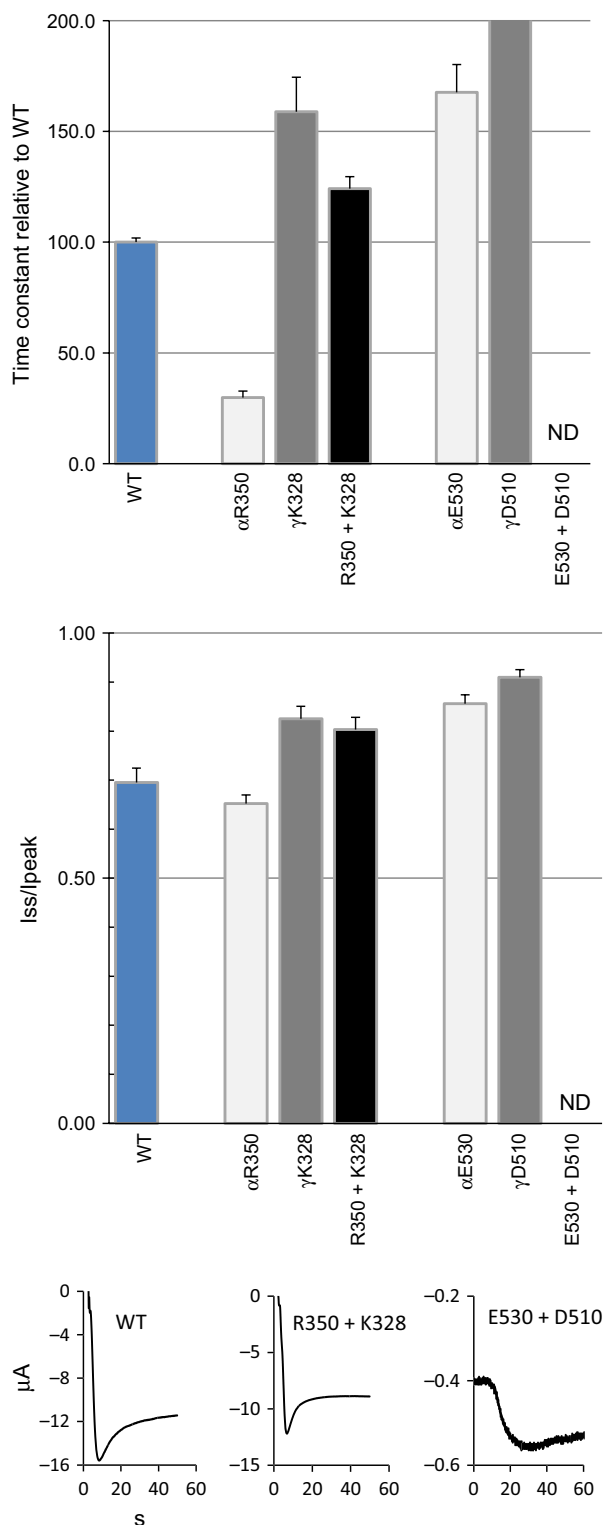
Fig. 10. SSI response in oocytes expressing α- and γ-ENaC subunits with homologous charged residues mutated to Ala. Oocytes were injected with WT cRNA for β-ENaC and α- and γ-ENaC cRNAs carrying a single residue mutated to Ala (WT without a mutation). For experimental details, see the legend to Fig. 7. The mean time constant value τ for oocytes co-expressing both mutated α- and γ-ENaC subunits (αR350 + γK328) was significantly different from the WT ($P < 0.001$). For I_{ss}/I_{peak} measurements, all mutants except αR350 were significantly different from WT ($P < 0.01$). In oocytes co-expressing mutated α- and γ-ENaC subunits with αE530 + γD510 mutations, the time constant value could not be measured because there was no detectable self-inhibition. Recordings show representative samples of current decay in these experiments.

subunit (Fig. 1 and Table 1). For each mutant, we assayed three parameters: (a) macroscopic Na$^+$ conductance; (b) the intensity of oocyte surface fluorescence of the α-ENaC–YFP hybrid as a measure of surface concentration; and (c) SSI response parameters.

The results showed a strong correlation ($r = 0.77$) between Na$^+$ conductance activity and oocyte surface density (Fig. 5). These results extend our previous observations with α-ENaC alanine mutagenesis [3] to the γ-subunit as well. By contrast to membrane fluorescence, SSI response parameters, τ and the I_{ss}/I_{peak} showed no correlation with Na$^+$ conductance.

The first concern with respect to mutating a specific residue is to determine whether the mutation disrupts the structure of the protein yielding a multitude of nonspecific effects resulting from major structural changes. As noted earlier, by selecting residues located on the protein surface, we limited the possibility of nonspecific effects on structure [3]. Moreover, the results summarized above revealed distinct effects of the mutants that are not consistent with nonspecific effects or the destruction of channel function.

Below, we present an analysis of the functional effects of the mutations based on our knowledge of ASIC1 structure [8]. In this analysis, we consider two structural aspects for each residue: (a) the secondary structural domain wherein the residue is located and (b) the relative surface location of residue. In the second aspect, we relate to the following positions: (a) residues on the solvent accessible surface but not on the interface between subunits; (b) residues at the interface between subunits; and (c) residues on a projected path of ion in the central vestibule [10].

Discussion

In the present study, we examined the roles of 17 conserved charged residues on the surface of the γ-ENaC

Structural locations of residues that affected the SSI response

Among 17 γ-ENaC residues mutated, only four (K328, D510, R514 and E518 mutants) showed a significant

effect on the time constant of the SSI response (Fig. 7). The importance of these residues for the SSI response is also confirmed by previous results on alanine mutagenesis of homologous residues in α-ENaC [3], as well as results on the co-expression of two of these α-ENaC mutants (R350 and E530) together with γ-ENaC mutants (Fig. 10).

The ASIC1 homologs of three of these residues (D510, R514 and E518) are located within or just before the β12 strand on the palm domain of ASIC1 (Fig. 1 and Table 1). This strand is connected to the carboxy-terminal trans-membrane domain (TM2) of ASIC1 that forms part of the channel pore [10]. The fourth residue of γ-ENaC (K328) is located in the β-ball domain. Mutations in this region have been shown to disrupt inter-subunit interfaces [5].

In the ASIC1 structure, the homologs of all four γ-ENaC residues (K328, D510, R514 and E518) are located at the interface between subunits (Table 2). Mutation of residues located on the exposed surface of ENaC (e.g. E255 and E336) (but not at subunit interface) did not show any significant effect on the self-inhibition response (Fig. 7 and Table 2). Similarly, in our previous study on α-ENaC, we observed that alanine mutagenesis of D400 and D446 located on α-ENaC surface showed no effect on self-inhibition parameters [3]. The residues that we selected for mutagenesis are located at highly conserved sites along the ENaC sequences. Such residues commonly appear at hot spots

of protein–protein interactions [27,28]. Based on these considerations, it is highly likely that the interface location of the homologous ASIC1 residues holds true for most, if not all, residues examined in the present study in α- and γ-ENaC. Thus, we conclude that the residues identified as being essential for the SSI response are probably located at the interface between ENaC subunits similar to their homologs in ASIC1 (Table 2).

A residue located at the interface between subunits may be fulfilling various roles [35,36]. It may participate in (a) stable protein–protein interactions between subunits or (b) transient protein–protein interactions between subunits that trigger regulatory conformational changes. In addition to these options, because ENaC is an ion channel, charged residues at the interface may be involved in binding ions that enter the channel vestibules. Below, we present an examination of these options for selected residues.

Positions and possible functions of γ-ENaC Arg514 and Glu518

To understand the functions of the residues identified in the present study, we concentrate on two of them: R514 and E518. These two were selected because they are located at a region that is highly conserved in all three ENaC subunits, as well as in ASIC1.

In aligned sequences, the ASIC1 homolog of Arg514 is Glu417. This glutamate of each of the three ASIC1

Table 2. Summary of the effects of α- and γ-ENaC alanine mutants on surface expression and SSI time constant τ.

Effect of mutation	α-ENaC residue	γ-ENaC residue	ASIC1 homolog	Buried area (%)[a]	ASIC1 location[b]
↓ Surface expression (SE)		K181	–		
		E255	E168	0	Surface
		E314	Q227	79–86	Interface
		E336	E255	0	Surface
		E445	E354	61–62	Interface
		E446	K355	39–41	Interface
		K498	–		
↓ Na$^+$ self-inhibition τ (SSI)		R514	E417	5–8	Central vestibule (Fig. 11)
		E518	Q421	46–53	Interface (Fig. 12)
↓ SE and ↓ SSI	R350	K328	K247	92–95	Interface
	E530	D510	A413	60–61	Interface
No effect		R178	–		
		D213	K142	0	Surface
		E254	–		
		E315	D228	1–5	Surface
		E316	E229	0	Surface
		D378	D297	0	Surface

[a]Percentage of accessible surface area of the residue buried between subunits, based on analysis of the structure of 2QTS [8] by PDBe PISA. In the ASIC1 homotrimer, there are three subunit interfaces: A–B, B–C and A–C. The values shown represent the range for these three interfaces. [b]Interface: buried between subunits. Central vestibule: located in the central vestibule [10]. Surface: exposed on protein surface.

subunits protrudes into the central vestibule along the central symmetry axis of ASIC1 (Fig. 11). Thus, these three glutamates form a triangular triad in center of the vestibule and have been implicated in proton binding and functional conformational changes in ASIC1 [8,37]. The contrast between ENaC and ASIC1 subunits is that, although the conserved residue is a negatively-charged Glu in ASIC1, in all three ENaC subunits, the homologous position is occupied by a positively-charged Arg or Lys in all of the available ENaC sequences. In the low pH structure of ASIC1, there is a continuous passageway of vestibules starting at the top of the trimer center and extending to the channel pore along the rotational axis of symmetry. This pathway is severely constricted before the central vestibule, although Gonzales *et al.* [10] suggest that, under physiological conditions, this central vestibule probably functions as a pathway for ions.

The ASIC1 homolog of Glu518 is Gln421. In ASIC1, Q421 directly participates in subunit–subunit interactions because it is hydrogen bonded to the side chain of D79 in the neighboring subunit (Fig. 12).
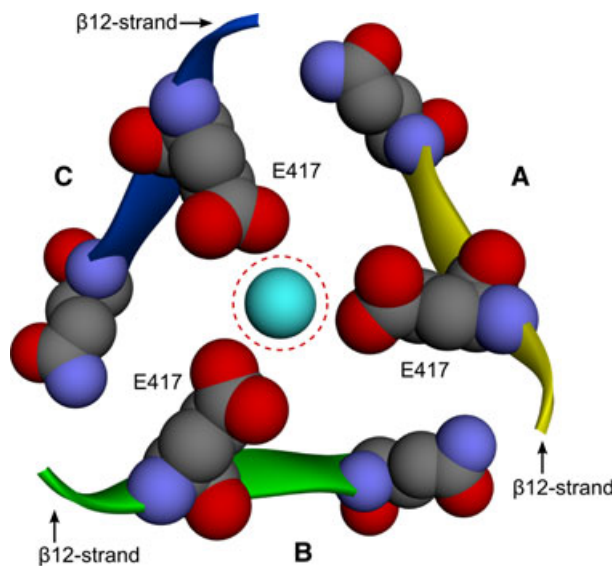

Fig. 11. Location of the γ-ENaC subunit R514 homolog E417 in the central vestibule of ASIC1. The three ribbon structures shown represent the β12-strand region (from L414 to K423) of all three subunits of chicken ASIC1, termed in order A, B and C (PDB 2QTS). For each subunit, only two residues, E417 and Q421, are shown in CPK style. In all human, mouse, rat and rabbit ENaC subunits, the residue homologous to E417 is an arginine or lysine (R514 in γ-ENaC and K534 in α-ENaC). The space in the center is part of the vestibule along the three-fold axis of symmetry that is assumed to be part of the ion pathway [10]. The blue sphere inside the dashed circle represents water molecule used by POREWALKER software to mark the tunnel (Fig. 1).
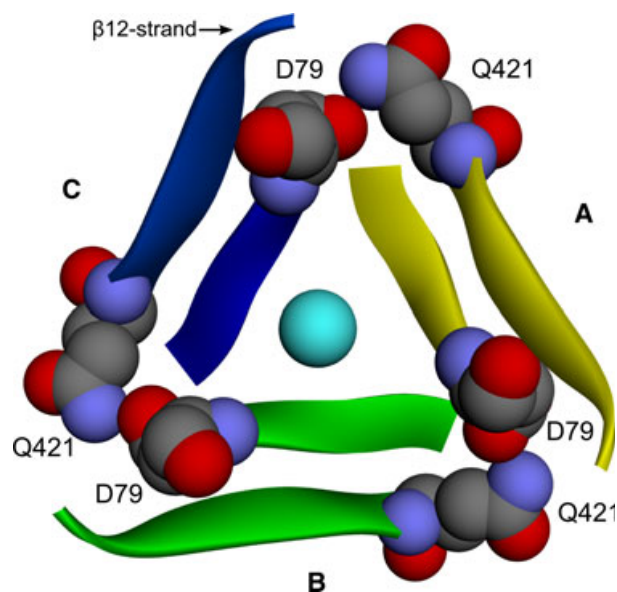

Fig. 12. Importance of the γ-ENaC subunit E518 homolog Q421 with respect to inter-subunit contact among the three subunits of ASIC1. The ribbon structures shown include the β12-strand region (from L414 to K423) and the β1-strand region (from H74 to E80) of all three subunits of chicken ASIC1, termed in order A, B and C. For each subunit, only two residues, D79 and Q421, are shown in CPK style. The N atom of Q421 is hydrogen bonded to the O atom of D79 side chain in the neighboring subunit. In all human, mouse, rat and rabbit ENaC subunits, the residue homologous to Q421 is a glutamate (E518 in γ-and E538 in α-ENaC) that is conserved in all human and mouse ENaC subunits.

Implications for the mechanism of the SSI response of ENaC

Extracellular Na^+-dependent self-inhibition is a mechanism of ligand inhibition of ENaC that prevents flooding of the cell with excess Na^+ ions [4,38]. ENaC type channels are constitutively active but an increase in the extracellular Na^+ concentration reduces channel conductance. The kinetics of SSI suggests that a dynamic conformational change in the ENaC structure constrains the channel within seconds after increased Na^+ flow. Because this response is steeply dependent on temperature, the inhibition should be much faster at body temperature than that observed under experimental conditions [22]. There is clinical evidence indicating that the self-inhibition response is an essential physiological response. In a patient with atypical cystic fibrosis, an α-ENaC W493R mutation was identified that resulted in constitutive activation of ENaC, apparently as a result of abolition of the extracellular Na^+ dependent self-inhibitory response of ENaC [39].

With our current understanding of the structure and function of the ENaC channel, there are at least two

features necessary for the ENaC site(s) initiating the SSI response: (a) it should sense an increased concentration of Na^+ ions by transient binding of ions and (b) it should be able transmit this information by a conformational change that leads to constriction of the channel. On the basis of the findings obtained in the present study, we suggest that the charged residues identified above, located on or before the β12-strand and exposed to solvent within the vestibules in the rotational symmetry axis of ENaC, are good candidates for this role (Figs 1, 11 and 12).

To explain the mechanism of gating in mechano-sensitive DEG type channels, it has been suggested that mechanical stimuli force the channel open as a result of extracellular matrix components tethered to the ectodomain of DEG subunits [5]. This extracellular effect is then hypothesized to move the TM domains embedded in the membrane, leading to the opening of the channel pore [5]. In proton-gated ASIC type channels, it has been suggested that proton binding in the ion channels moves the thumb and wrist regions, which in turn move the TMs opening the channel pore [10]. The common theme in both of these gating models is a conformational change in specific ectodomain structures that leads to a movement of the TM domains opening the channel pore [40].

Currently, we do not know whether the SSI response is a result of constriction of ENaC at TM domain levels, as in ASIC1 and DEG type channels, or at a site that precedes this ultimate pore level. Sections of this pathway are shown in Figs 1, 11 and 12. It is possible that the accumulation of Na^+ ions in this pathway causes a conformational change leading to a restriction of the channel at a level that precedes the TM domains.

Implications for the transport of ENaC subunits to the membrane

With human ENaC cDNAs, we showed that there is no detectable activity of ENaC, and surface expression of the two subunits alone is drastically reduced, without co-expression of all three subunits [3]. Thus, final delivery to the cell membrane and the assembly of functional ENaC is dependent on all three intact subunits. As summarized in Table 2, we observed that alanine mutagenesis of residues located at both the interface between the subunits and on the exposed surface of ENaC (e.g. E255 and E336 in γ-ENaC) can adversely affect the surface expression of ENaC. The three ENaC subunits are probably assembled in the endoplasmic reticulum (ER) [41] and are destined for transport to the cell surface via the trans-Golgi net-

work, as is typical for the trafficking of proteins in polarized epithelial cells [42]. One hypothesis for the effect of mutated residues at the subunit–subunit interface is that these residues represent focal points of subunit interaction during the assembly of the subunits prior to transport to the cell membrane.

Trafficking of proteins via the endoplasmic reticulum and trans-Golgi network involves a large number of sorting systems and transport carriers [21,42,43]. It is likely that, after trimeric ENaC is assembled, it is anchored to other proteins involved in the sorting and transport machinery. One of our hypotheses is that the mutated charged residues on the exposed surface of ENaC subunits may be anchor points for binding to such proteins during the transport process. Mutated ENaC subunits that do not assemble properly and do not reach surface are likely directed to endoplasmic reticulum associated degradation (ERAD) [44,45].

Another possibility to explain the reduced surface expression of the ENaC harboring a mutant residue is that the mutation may disrupt native protein folding, leading the protein into ERAD. We consider that alanine mutations do not lead to gross protein misfolding. (a) As noted above, we selected residues where the R group protrudes on the surface of the protein. Thus, the probability that, in such positions, alanine substitution leads to misfolding of the protein should be less than that for residues in the interior of the protein. (b) At the positions we studied, mutation of a residue at the same time as maintaining the charge of the residue leads to a protein that is functionally not different from WT [3]. This suggests that changes in the R group at these positions can be tolerated without leading to any major damage in ENaC function. (c) Immunoprecipitation of the α-ENaC subunits did not show any difference in the amounts of WT versus mutated proteins that could be indicative of a preferential degradation of similarly mutated α-ENaC subunits [3]. (d) The Na^+ conductance of ENaC containing a mutated subunit is proportional to the membrane concentration of ENaC (Fig. 5). If the mutation enhances the propensity of the protein for misfolding, then the activity of the channel should be much less than that relative to its surface concentration. For example, in the case of K328A mutant, membrane fluorescence is only 7% of WT, although conductance is 30% of WT (Fig. 5). Thus, in the case of this mutant, the mutation does not reduce the activity of ENaC relative to its surface level. In summary, in our view, the high correlation between conductance and fluorescence suggests that the reduced level of surface expression is mainly a result of an interruption in the process of the trafficking of ENaC, rather than the result of a misfolded

mutated protein. We hope that these mutants will prove useful in the analysis of the details of the trafficking of ENaC subunits in future research.

Conclusions

The results of the present study on alanine mutants of 17 conserved charged residues on the γ-ENaC surface showed that the Na$^+$ conductance of cells expressing these mutants can be accounted for by two parameters: (a) the ENaC concentration on cell surface as measured by the fluorescence of an α-ENaC–YFP hybrid and (b) the SSI response. Overall, the activity of all 17 mutants was correlated with the surface levels of ENaC. These findings confirm our previous results on α-ENaC and generalize these to γ-ENaC as well. There was no quantitative correlation between these parameters measured for α- and γ-ENaC mutants at nine homologous positions. Thus, the functions of most of the homologous surface residues examined differ between the two subunits. Only four mutants (K328, D510, R514 and E518) most significantly reduced the SSI time constant. The α-ENaC homologs of three of these residues (R350, E530 and E538) also severely affected the SSI response. These residues are located at a domain with conserved sequences in the ENaC and ASIC1 subunits and the behavior of these mutants can be explained by features of the ASIC1 structure. Homologous residues in ASIC1 are located at the interface between subunits and are located at positions on or about the ion pathway at the rotational symmetry axis in the center of the trimer. Thus, it is possible that these residues are involved in conformational changes that lead to channel constriction and the SSI response upon Na$^+$ ion flooding.

Materials and methods

Plasmids and site-directed mutagenesis

ENaC cDNA clones were generated from total human lung RNA as described previously [3]. To examine the function of conserved charged residues by site-directed mutagenesis, we selected 17 residues that are conserved in all known sequences of γ-ENaC from eight species (Fig. 1 and Table 1). These residues were modified to nonpolar alanine using our site-directed mutagenesis method [46] with the primers listed in Table 3. Table 3 includes only the forward primers. The reverse primers were complementary in sequence. After mutagenesis, we sequenced all isolated cDNAs using an ABI 310 Genetic Analyzer (Applied Biosystems, Foster City, CA, USA) to confirm that the cDNAs had the expected sequences without any additional change.

Electrophysiological measurements

The cDNAs were transcribed *in vitro* using T7-RNA polymerase (Promega, Madison, WI, USA) to generate cRNAs. The cRNAs (1 ng for each subunit) were micro-injected into immature stage V–VI *Xenopus* oocytes that were dissociated with 0.3 mg·mL^{-1} type 1A collagenase. The oocytes were incubated at 19 °C in ND-96 medium (in mM: 96 NaCl, 2 KCl, 1 CaCl$_2$, 1 MgCl$_2$ and 5 Hepes, pH 7.4) containing 2.5 mM sodium pyruvate, 50 μg·mL^{-1} gentamicin and 10 μM amiloride. After incubation for 24 h, the oocytes were transferred to NaCl-1 medium (ND-96 medium with

Table 3. Forward primers used for mutation of charged residues to alanine by site-directed mutagenesis.

	Mutation	Primer (5′- to 3′)
1	Arg178Ala	GACTTCTTCACAGGGGCGAAGCGGAAAGTCGGC
2	Lys181Ala	CACAGGGAGGAAGCGGGCAGTCGGCGGTAGCATC
3	Asp213Ala	CTCAAATGACACCTCCGCCTGTGCCACCTACACC
4	Glu254Ala	CATGAGCTATTCTGCTGCGGAGCTGCTGGTGACC
5	Glu255Ala	GAGCTATTCTGCTGAGGCGCTGCTGGTGACCTGC
6	Glu314Ala	GTACATAAACGCAGAGGAATACAACCCATTC
7	Glu315Ala	GTACATAAACGAAGCGGAATACAACCCATTC
8	Glu316Ala	CATAAACGAAGAGGCATACAACCCATTCCTC
9	Lys328Ala	CCTCCACTGGAGCTGCGGTGATCATCCATCGG
10	Glu336Ala	CATCCATCGGCAGGATGCGTATCCCTTCGTCGAAG
11	Asp378Ala	CCGATGGATGATCACCGCAGCTCCAGTGGAGG
12	Glu445Ala	CGAGCCTTTGTCCAGGCAGAGCTGGGCTGCCAG
13	Glu446Ala	GCCTTTGTCCAGGAAGCGCTGGGCTGCCAGTCTG
14	Lys498Ala	CAAAAAGCTCAACGCGACAGACTTGGCCAAAC
15	Asp510Ala	GATATTCTACAAAGCCCTGAACCAGAGATCC
16	Arg514Ala	CAAAGACCTGAACCAGGCATCCATCATGGAGAGC
17	Glu518Ala	CAGAGATCCATCATGGCGAGCCCAGCCAACAG

1 mM NaCl and 95 mM *N*-methyl-D-glucamine instead of 96 mM NaCl) and, 30 min later, the measurements were carried out using the two-electrode voltage-clamp method, where the oocytes were clamped at −60 mV. After the initiation of the clamp, current was recorded in three conditions with the sequence: (a) basal current for 1 min in NaCl-1 medium; (b) Na^+ current for 2 min after switching perfusion medium to NaCl-33 medium (in mM: 33 NaCl, 2 KCl, 1 $CaCl_2$, 1 $MgCl_2$, 5 Hepes, pH 7.4, 63 *N*-methyl-D-glucamine); and (c) amiloride-inhibited basal current for 1 min after switching perfusion medium to ND-96 + 10 μM amiloride. SSI response parameters, τ and I_{ss}/I_{peak}, were determined as described previously [3,25,33]. Because this response is strongly dependent on temperature [22], all the experiments were carried out at room temperature maintained at 22 °C.

Data were collected and analyzed using PCLAMP software (Axon Instruments, Foster City, CA, USA).

Fluorescence measurements and detection of YFP expression in oocytes

To examine the oocyte membrane distribution of ENaC subunits, we generated an α-ENaC-fluorescent protein fusion construct. For this, we amplified the coding region of the YFP and inserted the PCR fragment at the *Bam*HI site after the α-ENaC coding sequence in PGEM-HJ vector.

In experiments designed to determine the fluorescence of α-ENaC–YFP hybrid protein in oocyte membrane, 3 ng of cRNA was injected into oocytes. The oocytes were incubated in ND-96 medium with 10 μM amiloride at 19 °C for 3 days. The oocytes were then transferred with a pipette to ND96 medium in 0.7-mm glass-bottom dish for imaging using a confocal fluorescence microscope (LSM 510 META; Zeiss, Jena, Germany) with either ×5 or ×20 air objectives. YFP fluorescence was excited using a 514 nm argon laser line. Emission spectrum was recorded with a filter in the range 524–609 nm.

Intensity of YFP fluorescence showed no significant variation along the border of the animal (dark) hemisphere. For each oocyte, the fluorescence intensity was taken as the mean of three points on the membrane, minus the average of three points inside the dark (nontransparent) part of the animal hemisphere using LSM IMAGE EXAMINER software, version 4.2 (Zeiss).

Statistical analysis

The activity of each mutant cRNA was tested in at least two independent experiments with at least 10 oocytes. Measurements were carried out without knowledge of the injected cRNA. Significance of the difference between means was analyzed first by one-way analysis of variance. Significance of the difference for subsequent multiple comparisons between each mutant group versus the control

WT sample mean was tested by Dunnett's test using GRAPHPAD INSTAT, version 3.00 (GraphPad Software, San Diego, CA, USA).

Software for analysis of sequence and structure

Multiple sequence alignment for the identification of conserved or homologous residues was carried out using CLUSTAL software [47]. Clustal results were visualized using GENEDOC (http://www.nrbsc.org/gfx/genedoc/) [48]. Structural comparisons between human α-ENaC and ASIC1 model [8] were limited only to regions showing unequivocal sequence homology. Molecular models were visualized using DISCOVERY STUDIO VISUALIZER (Accelrys, San Diego, CA, USA). Solvent accessible surface residues and residues at the interface between ASIC1 subunits were determined using the PISA web server for the exploration of macromolecular interfaces located at PDBe [49]. The longest cavity that may serve as an ion pore in ASIC1 was identified using POREWALKER [50]. Structural graphics were generated using DISCOVERY STUDIO (Accelrys).

Acknowledgements

References

1 Kellenberger S & Schild L (2002) Epithelial sodium channel/degenerin family of ion channels: a variety of functions for a shared structure. *Physiol Rev* **82**, 735–767.

2 Enuka Y, Hanukoglu I, Edelheit O, Vaknine H & Hanukoglu A (2012) Epithelial sodium channels (ENaC) are uniformly distributed on motile cilia in the oviduct and the respiratory airways. *Histochem Cell Biol* **137**, 339–353.

3 Edelheit O, Hanukoglu I, Dascal N & Hanukoglu A (2011) Identification of the roles of conserved charged residues in the extracellular domain of an epithelial sodium channel (ENaC) subunit by alanine mutagenesis. *Am J Physiol Renal Physiol* **300**, F887–F897.

4 Kashlan OB & Kleyman TR (2011) ENaC structure and function in the wake of a resolved structure of a family member. *Am J Physiol Renal Physiol* **301**, F684–F696.

5 Eastwood AL & Goodman MB (2012) Insight into DEG/ENaC channel gating from genetics and structure. *Physiology (Bethesda)* **27**, 282–290.

6 Ben-Shahar Y (2011) Sensory functions for degenerin/epithelial sodium channels (DEG/ENaC). *Adv Genet* **76**, 1–26.

7 Saxena A, Hanukoglu I, Strautnieks SS, Thompson RJ, Gardiner RM & Hanukoglu A (1998) Gene structure of the human amiloride-sensitive epithelial sodium channel beta subunit. *Biochem Biophys Res Commun* **252**, 208–213.

8 Jasti J, Furukawa H, Gonzales EB & Gouaux E (2007) Structure of acid-sensing ion channel 1 at 1.9 Å resolution and low pH. *Nature* **449**, 316–323.

9 Baconguis I & Gouaux E (2012) Structural plasticity and dynamic selectivity of acid-sensing ion channel-spider toxin complexes. *Nature* **489**, 400–405.

10 Gonzales EB, Kawate T & Gouaux E (2009) Pore architecture and ion sites in acid-sensing ion channels and P2X receptors. *Nature* **460**, 599–604.

11 Collier DM & Snyder PM (2011) Identification of epithelial Na^+ channel (ENaC) intersubunit Cl-inhibitory residues suggests a trimeric alpha gamma beta channel architecture. *J Biol Chem* **286**, 6027–6032.

12 Chang SS, Grunder S, Hanukoglu A, Rösler A, Mathew PM, Hanukoglu I, Schild L, Lu Y, Shimkets RA, Nelson-Williams C *et al.* (1996) Mutations in subunits of the epithelial sodium channel cause salt wasting with hyperkalaemic acidosis, pseudohypoaldosteronism type 1. *Nat Genet* **12**, 248–253.

13 Saxena A, Hanukoglu I, Saxena D, Thompson RJ, Gardiner RM & Hanukoglu A (2002) Novel mutations responsible for autosomal recessive multisystem pseudohypoaldosteronism and sequence variants in epithelial sodium channel alpha-, beta-, and gamma-subunit genes. *J Clin Endocrinol Metab* **87**, 3344–3350.

14 Hanukoglu A, Edelheit O, Shriki Y, Gizewska M, Dascal N & Hanukoglu I (2008) Renin-aldosterone response, urinary Na/K ratio and growth in pseudohypoaldosteronism patients with mutations in epithelial sodium channel (ENaC) subunit genes. *J Steroid Biochem Mol Biol* **111**, 268–274.

15 Edelheit O, Hanukoglu I, Gizewska M, Kandemir N, Tenenbaum-Rakover Y, Yurdakök M, Zajaczek S & Hanukoglu A (2005) Novel mutations in epithelial sodium channel (ENaC) subunit genes and phenotypic expression of multisystem pseudohypoaldosteronism. *Clin Endocrinol* **62**, 547–553.

16 Edelheit O, Hanukoglu I, Shriki Y, Tfilin M, Dascal N, Gillis D & Hanukoglu A (2010) Truncated beta epithelial sodium channel (ENaC) subunits responsible for multi-system pseudohypoaldosteronism support partial activity of ENaC. *J Steroid Biochem Mol Biol* **119**, 84–88.

17 Canessa CM, Schild L, Buell G, Thorens B, Gautschi I, Horisberger JD & Rossier BC (1994) Amiloride-sensitive epithelial Na^+ channel is made of three homologous subunits. *Nature* **367**, 463–467.

18 Rossier BC, Pradervand S, Schild L & Hummler E (2002) Epithelial sodium channel and the control of

sodium balance: interaction between genetic and environmental factors. *Annu Rev Physiol* **64**, 877–897.

19 Bader M (2010) Tissue renin–angiotensin–aldosterone systems: targets for pharmacological therapy. *Annu Rev Pharmacol Toxicol* **50**, 439–465.

20 Palmer LG, Patel A & Frindt G (2012) Regulation and dysregulation of epithelial Na^+ channels. *Clin Exp Nephrol* **16**, 35–43.

21 Kashlan OB & Kleyman TR (2012) Epithelial Na(+) channel regulation by cytoplasmic and extracellular factors. *Exp Cell Res* **318**, 1011–1019.

22 Chraibi A & Horisberger JD (2002) Na self inhibition of human epithelial Na channel: temperature dependence and effect of extracellular proteases. *J Gen Physiol* **120**, 133–145.

23 Sheng S, Maarouf AB, Bruns JB, Hughey RP & Kleyman TR (2007) Functional role of extracellular loop cysteine residues of the epithelial Na^+ channel in Na^+ self-inhibition. *J Biol Chem* **282**, 20180–20190.

24 Maarouf AB, Sheng N, Chen J, Winarski KL, Okumura S, Carattino MD, Boyd CR, Kleyman TR & Sheng S (2009) Novel determinants of epithelial sodium channel gating within extracellular thumb domains. *J Biol Chem* **284**, 7756–7765.

25 Sheng S, Carattino MD, Bruns JB, Hughey RP & Kleyman TR (2006) Furin cleavage activates the epithelial Na+ channel by relieving Na+ self-inhibition. *Am J Physiol Renal Physiol* **290**, F1488–F1496.

26 Guharoy M & Chakrabarti P (2010) Conserved residue clusters at protein–protein interfaces and their use in binding site identification. *BMC Bioinformatics* **11**, 286.

27 Halperin I, Wolfson H & Nussinov R (2004) Protein–protein interactions; coupling of structurally conserved residues and of hot spots across interfaces. Implications for docking. *Structure* **12**, 1027–1038.

28 Zhao N, Pang B, Shyu C-R & Korkin D (2011) Charged residues at protein interaction interfaces: unexpected conservation and orchestrated divergence. *Protein Sci* **20**, 1275–1284.

29 Li J, Sheng S, Perry CJ & Kleyman TR (2003) Asymmetric organization of the pore region of the epithelial sodium channel. *J Biol Chem* **278**, 13867–13874.

30 Shi S, Carattino MD & Kleyman TR (2012) Role of the wrist domain in the response of the epithelial sodium channel to external stimuli. *J Biol Chem* **287**, 44027–44035.

31 Hughey RP, Bruns JB, Kinlough CL, Harkleroad KL, Tong Q, Carattino MD, Johnson JP, Stockand JD & Kleyman TR (2004) Epithelial sodium channels are activated by furin-dependent proteolysis. *J Biol Chem* **279**, 18111–18114.

32 Kleyman TR, Carattino MD & Hughey RP (2009) ENaC at the cutting edge: regulation of epithelial sodium channels by proteases. *J Biol Chem* **284**, 20447–20451.

33 Sheng S, Bruns JB & Kleyman TR (2004) Extracellular histidine residues crucial for Na+ self-inhibition of epithelial Na$^+$ channels. *J Biol Chem* **279**, 9743–9749.

34 Sheng S, Perry CJ & Kleyman TR (2002) External nickel inhibits epithelial sodium channel by binding to histidine residues within the extracellular domains of alpha and gamma subunits and reducing channel open probability. *J Biol Chem* **277**, 50098–50111.

35 Nooren IMA & Thornton JM (2003) Diversity of protein–protein interactions. *EMBO J* **22**, 3486–3492.

36 Ozbabacan SEA, Engin HB, Gursoy A & Keskin O (2011) Transient protein–protein interactions. *Protein Eng Des Sel* **24**, 635–648.

37 Ishikita H (2011) Proton-binding sites of acid-sensing ion channel 1. *PLoS One* **6**, e16920.

38 Bize V & Horisberger JD (2007) Sodium self-inhibition of human epithelial sodium channel: selectivity and affinity of the extracellular sodium sensing site. *Am J Physiol Renal Physiol* **293**, F1137–F1146.

39 Rauh R, Diakov A, Tzschoppe A, Korbmacher J, Azad AK, Cuppens H, Cassiman JJ, Dotsch J, Sticht H & Korbmacher C (2010) A mutation of the epithelial sodium channel associated with atypical cystic fibrosis increases channel open probability and reduces Na$^+$ self inhibition. *J Physiol* **588**, 1211–1225.

40 Li T, Yang Y & Canessa CM (2011) Outlines of the pore in open and closed conformations describe the gating mechanism of ASIC1. *Nat Commun* **2**, 399.

41 Buck TM, Plavchak L, Roy A, Donnelly BF, Kashlan OB, Kleyman TR, Subramanya AR & Brodsky JL (2013) The Lhs1/GRP170 chaperones facilitate the endoplasmic reticulum-associated degradation of the epithelial sodium channel. *J Biol Chem* **288**, 18366–18380.

42 Cao X, Surma MA & Simons K (2012) Polarized sorting and trafficking in epithelial cells. *Cell Res* **22**, 793–805.

43 Apodaca G, Gallo LI & Bryant DM (2012) Role of membrane traffic in the generation of epithelial cell asymmetry. *Nat Cell Biol* **14**, 1235–1243.

44 Buck TM, Kolb AR, Boyd CR, Kleyman TR & Brodsky JL (2010) The endoplasmic reticulum-associated degradation of the epithelial sodium channel requires a unique complement of molecular chaperones. *Mol Biol Cell* **21**, 1047–1058.

45 Tamura T, Sunryd JC & Hebert DN (2010) Sorting things out through endoplasmic reticulum quality control. *Mol Membr Biol* **27**, 412–427.

46 Edelheit O, Hanukoglu A & Hanukoglu I (2009) Simple and efficient site-directed mutagenesis using two single-primer reactions in parallel to generate mutants for protein structure–function studies. *BMC Biotechnol* **9**, 61.

47 Chenna R, Sugawara H, Koike T, Lopez R, Gibson TJ, Higgins DG & Thompson JD (2003) Multiple sequence alignment with the Clustal series of programs. *Nucleic Acids Res* **31**, 3497–3500.

48 Nicholas KB & Deerfield DW II (1997) GeneDoc: analysis and visualization of genetic variation. *EMBnet.news* **4**, 1–4.

49 Krissinel E & Henrick K (2007) Inference of macromolecular assemblies from crystalline state. *J Mol Biol* **372**, 774–797.

50 Pellegrini-Calace M, Maiwald T & Thornton JM (2009) PoreWalker: a novel tool for the identification and characterization of channels in transmembrane proteins from their three-dimensional structure. *PLoS Comput Biol* **5**, e1000440.